Binocular modulation of monocular V1 neurons

Kacie Dougherty°, Michele A. Cox°, Jacob A. Westerberg, Alexander Maier*

Department of Psychology, College of Arts and Science, Vanderbilt Vision Research Center, Center for Integrative and Cognitive Neuroscience, Vanderbilt University, Nashville, TN 37203

°These authors contributed equally to this work.

*To whom correspondence should be mailed to at: alex.maier@vanderbilt.edu

KEYWORDS

binocular vision, binocular combination, binocular summation, binocular integration, cortical column, ocular dominance

ABSTRACT

Our brains combine the separate streams of sensory signals from the two eyes into a singular view. Where the separate streams from the two eyes first converge in the primary visual pathway is unclear. At the initial stage of visual processing following transduction in the retina, neurons in the lateral geniculate nucleus of the thalamus (LGN) are deemed monocular because they are excited by stimulation of one eye and not the other. At the next stage of visual processing, in the primary visual cortex (V1), there are many neurons that are deemed binocular because they are excited by stimulation of either eye, signifying that binocular convergence has happened by that stage. Visual stimulation evokes a specific sequence of activation across the laminar microcircuit of V1. During which part of this sequence binocular convergence occurs is unresolved. Here we investigate where binocular convergence occurs in the V1 laminar microcircuit by examining the extent to which macaque V1 neurons in all layers are sensitive to both eyes. We found that more than 94% of V1 neurons across all layers were binocular in the sense that they were driven by stimulation of either eye. As expected, monocular neurons were largely located in the primary geniculate input layer of V1. Interestingly, these monocular neurons showed systematic firing rate differences between stimulation of their driving eye alone compared to stimulation of both eyes, revealing that these so-called monocular neurons actually encode what is shown to both eyes. This finding suggests that, while geniculate inputs to V1 are largely segregated by eye, the outputs of their V1 target neurons are sensitive to what both eyes view, marking this processing stage as the primary point of binocular convergence in the primate visual system.

INTRODUCTION

Front-facing eyes are one of the most prominent features that differentiate humans and other primates from their closest ancestors[1]. The resulting overlap of the two eyes' perspectives necessitates that our brains combine the outputs of the two eyes in order to yield a singular view of the visual field[2-14]. In order to be combined, the two signal streams of the eyes need to get in touch, or converge, at some point along the primary visual pathway. Where binocular convergence occurs on the level of single neurons is not entirely clear: Primate retinae do not receive feedback from the visual structures to which they project[15], which suggests that each eye's output is separate from that of the other eye. The main projection target of retinal ganglion cells is the lateral geniculate nucleus of the thalamus (LGN)[16]. Almost all primate LGN neurons are unaffected by stimuli in one of the two eyes[17], suggesting that binocular convergence occurs at a subsequent processing stage. The LGN mainly projects to the primary visual cortex (V1)[16], and the majority of V1 neurons are excited when a stimulus is presented to either eye[18,19]. These observations combined suggest that the main point of binocular convergence lies within V1, but the exact locus within the cortical microcircuit is unclear.

V1 is comprised of anatomically and physiologically distinct layers that are activated in a specific sequence following visual stimulation[20,21]. Binocular convergence occurs during one or more of these laminar activation steps, but which layers it occurs in is unclear. LGN neurons provide the sole geniculate input to individual neurons in layer 4C[22] . Given this connectivity, monocular signals might remain segregated within layer 4C and binocular convergence occurs during a subsequent step such as when these monocular layer 4C neurons project to neurons in layer 2/3[22]. Indeed, many layer 4C neurons are deemed monocular since they respond to one eye only[19,23]. Yet, these layer 4C stellate cells also receive inputs from other cortical neurons in

addition to the monocular inputs from the LGN[24,25]. These intracortical connections raise the alternative possibility that layer 4C neurons receive signals that correspond to either eye, yielding a de-segregated, binocular signal in this layer. While monocular neurons are driven (excited or suppressed) by one eye only, these neurons could still systematically change their firing rates when the other eye is stimulated as well. This phenomenon, termed binocular modulation, enables even so-called monocular neurons to encode what is shown to both eyes.

To our knowledge, no study to date has explicitly tested for binocular modulation of monocular layer 4C neurons in the awake primate. Stimulating both eyes simultaneously at corresponding retinal locations can be challenging. Occluding one eye in order to exclusively stimulate the other, for example, induces short-term plasticity[26] and involves an imbalance of overall luminance levels between monocular and binocular stimulation conditions. However, by using a mirror stereoscope, it is possible to circumvent these issues and stimulate each eye in isolation, or both eyes simultaneously, while keeping the overall level of luminance constant in both eyes.

Here we determine whether binocular convergence occurs in layer 4C or in adjacent layers, by examining the extent to which neurons in all layers of V1 are sensitive to one or both eyes. To do so, we employed linear multielectrode arrays to record V1 laminar neural responses in macaques that viewed stimuli with one eye, the other eye or both eyes through a custom-designed stereoscope. We found that almost 95% of V1 neurons across all layers were driven to some degree when stimuli were presented to either eye. Using a quantitative index of ocular dominance, we found that selectivity for the two eyes across all V1 neurons follows a normal distribution, while the degree to which neurons preferred one eye over the other varied systematically between layers. In line with earlier work, we located the bulk of monocular

spiking activity in layer 4C. Strikingly, we found that, although these neurons were only activated by one eye, these so-called monocular neurons were nonetheless sensitive to both eyes as their responses changed significantly when both eyes were stimulated simultaneously. In other words, V1 neurons across all layers were sensitive to not one but both eyes. These findings combined suggest that the primary point of convergence of the signals of the two eyes lies in the geniculo-recipient layers of V1.

RESULTS

Our primary objective in this study was to determine the extent to which neurons across V1 layers are sensitive to binocular inputs. Each day, we penetrated the *dura mater* over V1 with a linear multielectrode array and positioned the array so that its contacts spanned the depth of cortex. We displayed monocular and binocular visual stimuli through a mirror stereoscope to stimulate the left and right eyes independently. After mapping the receptive field (RF) location for the neurons under study (see **Methods** for details and an assessment of RF overlap across layers), we presented static sine-wave grating stimuli to the left eye or right eye over the RF location while the animals fixated on a central fixation cross (**Figure 1a**). We extracted well-isolated single units as well as multiunit activity (see **Methods**).

V1 ocular dominance distribution

We first determined the extent to which V1 neurons as a population were excited by visual stimulation of either eye. On most days, we recorded multiple single units across the cortical depth of V1 (**Figure 1b**). Over 45 recording sessions and 48 electrode penetrations, we isolated 207 single units from two macaques (N = 154 neurons in subject E48, see **Methods** for

inclusion criteria). In these penetrations as well as in additional penetrations in which only population spiking could be recorded (N = 60), we also computed the multiunit activity for each electrode channel, with each electrode channel within V1's gray matter yielding one multiunit (N = 837 multiunits, 670 from monkey E48, see **Methods** for inclusion criteria). To quantify the relative amount of excitation to stimulation of the contralateral eye versus the ipsilateral eye, we calculated a quantitative ocularity index for each unit (see **Methods** for formula). An ocularity index of -1 corresponded to neurons exclusively driven through the ipsilateral eye, and an ocularity index of 1 corresponded to neurons driven exclusively through the contralateral eye. An ocularity index of 0 corresponded to equal responses evoked through either eye. In line with previous reports, we observed that the vast majority (195/207, or 94.20%) of neurons in V1 were driven to some degree through either eye (**Figure 1c**) (see **Discussion** for a direct comparison with previous methods for classifying ocularity). Only 12/207 neurons, or 5.80%, of neurons in our sample were completely monocular in the sense that they exhibited no statistically significant response following stimulus onset (paired t-test, $p > .01$) and no detectable response to one eye based on additional visual inspection (46/207 neurons, or 22.22%, in our sample had no significant response to the non-dominant eye as assessed with a paired t-test, ($\alpha = .01$), but 34 of these 46 neurons exhibited a visible response to the non-dominant eye – note that to be safe, the analyses below will be performed on both groups of neurons: using additional inspection a criterion as well as using statistical threshold alone).

V1 population profile of ocular dominance

The distribution of response selectivity for one eye over another (ocular dominance, or ocularity) across the entire single unit population was well described by a Gaussian (Chi-square

goodness-of-fit, χ^2 = 17.66, d.f. = 8, p = 0.02), truncated at -1 and 1 to encapsulate the numerical limits imposed by the ocularity index. We repeated this analysis for the multiunit responses, as these data provided a larger sample. Since multiunit responses reflect the activity of neurons up to 350 μm away[27], which is enough distance to bridge across neighboring ocular dominance columns[28-30], we expected multiunits to exhibit a stronger bias towards binocular responses. Indeed, the mean rectified ocularity indices for multiunits were lower than those for single units (one-tailed t-test, p = 2.96 x 10^{-14}, t_{1042} = 7.61). Nonetheless, the distribution of multiunit ocularity was also fit well by a truncated Gaussian (Chi-square goodness-of-fit, χ^2 = 104.37, d.f. = 9, p = 2.25 x 10^{-18}). This finding suggests that while there are some V1 neurons that are excited by one eye only, these monocular neurons are the least common class of all possible ocular dominance combinations. The vast majority of neurons in V1 are excited by stimulation of either eye, with the mode of V1 neurons responding equally to either eye.

Laminar profile of ocular dominance

We next determined the profile of ocular dominance across the cortical depth of V1. Using a variety of neurophysiological criteria, we functionally identified the bottom of layer 4C as well as the upper and lower bounds of cortex for each penetration with the linear multielectrode array (see **Methods**). We chose the bottom boundary between layer 4C and layer 5 to serve as our reference point (0.0 mm) and assigned cortical depths to each unit recorded on contacts above and below relative to this reference point (+ 0.1 mm/contact). We then determined ocular dominance as a function of cortical depth. Specifically, we calculated the mean rectified ocularity index of all neurons at each cortical depth as a measure of how much each neuron was driven through one or both eyes (**Figure 2a**). We eliminated data from 4

penetrations (all from E48) that we considered oblique relative to the top of cortex based on the fact that they included multiunits that strongly preferred one eye and the other eye (ocularity index above and below 0.4 and -0.4, respectively).

We observed that, on average, the most monocularly-biased spiking for both single units and multiunits was in layer 4C, as defined by the initial current sink evoked by visually-evoked responses to full field visual flashes (**Figure 2b**) and RF-limited sine-wave gratings (**Figure 2c**). The rectified ocularity indices of multiunits differed significantly between laminar compartments (one-way ANOVA, $F(2,771) = 53.23$, $p = 2.22 \times 10^{-22}$). Specifically, there was a significant difference between the mean ocularity index in supragranular and infragranular layers (Tukey's HSD post-hoc test, $p = 9.56 \times 10^{-10}$, $N_{supragranular} = 255$, $N_{infragranular} = 189$) as well as between granular and infragranular layers (Tukey's HSD post-hoc test, $p = 9.56 \times 10^{-10}$, $N_{granular} = 330$, $N_{infragranular} = 189$). There was no significant difference between supragranular and granular layers (Tukey's HSD post-hoc test, $p = 0.25$, $N_{supragranular} = 255$, $N_{granular} = 330$). However, if testing was limited to multiunits that were located well inside layer 4C (i.e., 0.1 to 0.4 mm, inclusively), there was a significant difference between supragranular and granular compartments as well (one-way ANOVA, $F(2,662) = 70.83$, $p = 1.32 \times 10^{-28}$; Tukey's HSD post-hoc test, $p = .0001$). For our single-unit samples, which provided less statistical power, there was no significant difference between laminar compartments at the $\alpha = .05$ level. However, there was a difference at the $\alpha = 0.1$ level (one-way ANOVA, $F(2,185) = 2.42$, $p = .09$). The mean difference in single unit ocularity between the infragranular and supragranular compartments also tested at the $\alpha = 0.1$ level (Tukey's HSD post-hoc test, $p = .086$, $N_{supragranular} = 50$, $N_{infragranular} = 40$**)**.

The finding of greater ocular dominance among layer 4C neurons is congruent with previous work[19,23] and can be explained by the fact that monocular geniculate inputs primarily

target this layer[16]. Overall the pattern of rectified ocularity indices across cortical depth was qualitatively comparable for multiunits and single units, with some divergence at the extreme upper and lower bounds, which might be due to the lower number of single unit sampled at these locations (**Figure 2a**). Note that, while most monocular neurons were in layer 4C, this layer also harbors neurons that are equally driven through either eye (25-75%: 0.19-0.65)

Binocular modulation of monocular neurons

As described above, only ~5.8% (12/207) of the neurons in our sample showed no detectable response during visual inspection and no statistically significant response to one eye. We were particularly interested to test whether the responses of such monocular neurons modulated under binocular viewing. To do so, we conducted a second experiment, where we varied the contrast levels of the stimuli shown to the dominant eye, while holding stimulus contrast constant in the non-dominant eye. All other parameters were identical to our first experiment (**Figure 3a**). We performed a control condition of monocular stimulation, where we varied the contrast of the grating presented to the dominant eye from presentation-to-presentation (0%-no stimulus, 22.5%, 45%, and 90%), while keeping the non-dominant eye at mean luminance. For binocular stimulation, we varied contrast in the dominant eye in the same way as we did for monocular stimulation, while we presented a high contrast grating (90%) of identical orientation, phase and spatial frequency at the matching retinotopic position to the non-dominant eye.

For this second experiment, we recorded from a total of 77 neurons (N = 69 in E48). We then focused our analysis on monocular neurons only. To identify monocular neurons, we first considered those neurons that lacked a significant response to a visual stimulus in the non-

dominant eye (paired t-test, $p > 0.01$). We then split these neurons into a conservative and a liberal group. For the conservative group, we visually inspected the average responses to the non-dominant eye for this entire population, and further eliminated any neurons that exhibited any deflection from baseline, even though these deflections did not reach significance. Using this strict criterion, we identified 7 completely monocular neurons (*conservative group*, N = 6 from E48). To test our hypothesis with an increased sample size, we also used a more liberal criterion by including neurons from the conservative group as well as all neurons that both lacked a significant response to the non-dominant eye and had a rectified ocularity index above 0.65, regardless of whether visual inspection suggested a residual (non-significant) response or not (**Table 1**). This selection resulted in 16 monocular neurons (*liberal group*, N = 13 from E48).

Following this classification step, we tested whether these monocular neurons exhibited modulated responses under binocular stimulation. To do so, we first compared their responses between high contrast binocular stimulation and monocular stimulation of the dominant eye. Performing this comparison on an example single unit (**Figure 3b**) revealed that responses were suppressed under binocular stimulation relative to monocular stimulation during the first 100 ms of the response period (one-tailed t-test, $t_{47} = 1.56$, $p = 0.06$). The average response of the conservative group of monocular neurons showed the same response pattern (**Figure 3c, bottom**), in that their responses were significantly suppressed under binocular stimulation relative to monocular stimulation in the initial portion of the response (one-tailed t-test, $t_{12} = 2.59$, $p = 0.012$). All but one of the individual neurons showed significant differences throughout several time points in the response window (**Figure 3c, top**) (bootstrapped receiver operating characteristic (ROC) analysis, $p<0.05$, **see Methods**). Similar to the conservative group, the average response of the liberally defined group of monocular neurons was suppressed under

binocular stimulation relative to monocular stimulation (one-tailed t-test, $t_{30} = 1.77$, $p = 0.043$) (**Figure 3d, bottom**). All liberally defined neurons that were not already captured by the conservative definition showed significant differences throughout several time points in the response window (**Figure 3d, top**) (bootstrapped receiver operating characteristic (ROC) analysis, $p<0.05$, **see Methods**).

We next compared the contrast response functions of these monocular neurons during monocular stimulation and binocular stimulation (**Figure 3e-g**). This analysis revealed that the average response of the monocular neurons tended to be greater under binocular stimulation compared to monocular stimulation for low stimulus contrasts (22.5%), while showing significant suppression at high contrast levels relative to monocular stimulation ($p < 0.05$, same statistical tests as for Figures 3b-d) throughout the initial portion of the visual response. This difference between monocular and binocular responses of monocular V1 neurons was corroborated by an ROC analysis on the single unit level, which indicated that the maximum area under the curve for each neuron was above chance level (0.5) (**Figure 3h**, see also **Supplementary Figure 1b**). This finding is somewhat reminiscent of psychophysical findings, which similarly suggest that the outcome of binocular summation differs drastically between low and high contrast stimuli[2]. One reason for this difference might be that the brain uses a more additive approach for combining the two eyes' signals at low contrast levels in order to increase visual sensitivity. Attenuating the strength of both monocular inputs at higher contrasts in turn might help to normalize contrast perception between monocular and binocular viewing (as indicated by the fact that despite the virtual doubling of inputs, vision hardly changes between one and two eyes open).

Previous work as well as our first experiment predict monocular neurons to be primarily be in layer 4C. Indeed, for our conservative group, 5 of 7 monocular neurons were found in layer 4C (2 in layers 5/6). In our liberal group, 8 out of 16 neurons were in layer 4C (**Figure 3i**). In other words, the majority of monocular neurons was harbored by layer 4C, but monocular neurons were not exclusive to layer 4C.

We performed three control analyses to confirm that the binocular modulation of monocular neurons we observed was not the result of external, physical influences. First, to ensure that binocular modulation was not tied to eye movement-related activity, we chose to exclude any trials in which fixational eye movements (microsaccades) could be detected (see **Methods**). The main result of binocular suppression of monocular neurons held up after excluding trials with any fixational eye movements (one-tailed t-test, $t_{12} = 2.45$, $p = 0.015$) (**Suppl. Fig. 1**). Second, to ensure that we were stimulating the receptive field-matched position in the non-dominant eye, we analyzed the responses of other (binocular) single units recorded on other electrode contacts, simultaneously with the monocular neurons (**Figure 3j**). As expected, we observed visual responses for all those binocular neurons to both eyes, suggesting that the stereoscope and stimulus display worked correctly.

To summarize, across both experiments, we found evidence that although a small (~5-6%) proportion of neurons across all V1 layers are excited through one eye only, these neurons are nonetheless sensitive to the inputs to both eyes. This finding suggests that even geniculate-recipient layer 4C neurons, as well as all monocular V1 neurons in other layers, encode binocular information in that their firing rates are significantly altered when a stimulus is shown to their dominant eye alone or the non-dominant eye as well. We conclude that V1 layer 4C neurons, and monocular neurons in adjacent layers, seem to serve as a first major processing stage

downstream of the two eyes where monocular signals interact with sensory information of the other eye.

DISCUSSION

This study is the first to our knowledge demonstrating that primate V1 neurons in all layers are sensitive to what is shown to both eyes, including the so-called monocular neurons in layer 4C that are believed to receive the bulk of geniculate projections. In other words, neurons across the entire cortical column, including layer 4C, encode what both eyes view (**Figure 4**). These results are fundamental to our understanding of binocular combination. Several impactful theoretical models on binocular vision rest on the idea that that monocular neurons are inhibited by activation of the neuron's non-dominant eye[12,13,.31-33], but empirical evidence has been lacking. Therefore, the empirical findings reported here have important implications for our understanding of binocular rivalry and disorders of binocular vision such as stereoblindness, diplopia, strabismus and amblyopia.

Relation to Previous Work

The findings reported here parallel similar observations in cats[34]. However, binocular convergence seems to be implemented differently in cats than in primates. Specifically, the cat LGN features anatomical connections between monocular layers in the LGN that are either absent or less prominent in primates. Accordingly, the vast majority of cat LGN cells modulate responses under binocular viewing, which is only the case for a small minority of LGN neurons in the macaque (see [35] for a more extensive discussion of species differences). However, in both cats and primates there seems to be systematic, columnar binocular processing in the main

geniculate input layer of primary visual cortex. This organization is likely analogous as rodents, who are phylogenetically closer to primates than cats do not feature systematic columnar ocular dominance in the binocular zone of their primary visual cortex.

Previous work determined the fraction of primate V1 cells that are sensitive to one or both the eyes, and some considered ocularity across cortical depth[19]. Several of these studies used a scale to rate the extent to which neurons are driven more through one eye or the other[14,36,37]. This scale was composed of seven distinct groups, with groups 1 and 7 corresponding to neurons driven exclusively by the contra- and ipsilateral eyes, respectively, and group 4 corresponding to neurons driven equally through both eyes. Using this technique, some authors reported distributions appearing Gaussian[14] , which matches our finding based on a more quantitative approach. However, others reported distributions appearing closer to uniform[37]. Reasons for this variance might include the subjective nature of the rating system and the laminar position of neurons sampled. Importantly, though, there is wide agreement between previous studies and our finding that only a small fraction of V1 neurons is monocular[38].

Binocular Convergence in V1 Layer 4C

The binocular response modulation of monocular neurons we observed could arise through one of several mechanisms or a combination thereof. First, geniculate projections to V1 layer 4C do not exclusively target neurons in the ocular dominance column of one eye[39]. Instead, some geniculate axons bifurcate to innervate neighboring ocular dominance columns and might form—possibly less potent—connections with neurons in intermediate ocular dominance columns for the other eye. Second, intralaminar interactions among neurons within layer 4C, including those by bridging interneurons, would allow for cross-talk between the signals

encoding the output of each eye if these interneurons cross ocular dominance columns[24,40]. Lastly, inter-laminar projections targeting 4C neurons from excitatory and inhibitory neurons in other layers, most prominently from layer 6 might feed binocular signals back to monocular cells in layer 4C[41]. The latter loop is particularly interesting as layer 6 cells mainly target smooth and sparsely spiny stellate cells in layer 4, which are thought to be inhibitory[42]. The latter case would imply that binocular combination in the form of intracellular summation of monocular synaptic inputs from either eye to suprathreshold (spiking) activity occurs outside layer 4C and binocular response modulation of layer 4C monocular neurons is secondary to binocular combination within binocular neurons. However, there are several theoretical and psychophysical studies that suggest that monocular signals likely interact on the level of monocular neurons before these signals get combined in order to achieve interocular contrast normalization (a process related to the fact that our visual perception hardly changes between one or both eyes open). This theoretical prediction is further corroborated by human fMRI[43]. The most parsimonious conclusion given these previous reports is that the primary visual pathway contains monocular neurons that interact before binocular combination occurs. Our study suggests that these kinds of interactions primarily occur in layer 4C of V1 (see below).

Binocular Modulation in the LGN

Another important consideration is that monocular neurons in the LGN may exhibit a similar pattern of binocular modulation as monocular neurons in V1. Indeed, as discussed above, there is extensive work in cats demonstrating that while virtually all LGN neurons are excited by one eye only, most LGN neurons modulate responses to this dominant eye when a stimulus is shown to the other eye as well. Cat cortical inactivation studies aimed at delineating whether this

binocular modulation is fed back from visual cortex or computed locally within the LGN produced equivocal results[44-48]. Importantly, however, the fraction of primate LGN cells that modulate their visual responses between monocular and binocular stimulation is much smaller than that reported in the cat, and these neurons may be specific to the magnocellular subsystem of primate LGN[49]. Whether these responses are inherited via feedback from V1 has never been tested in the primate. Interestingly, it was recently found that a small fraction of primate LGN neurons responds to either eye[50,51]. These neurons comprise a small subsection of the koniocellular neurons in the LGN. Whether these binocular responses are supported by local neural interactions is unknown as these responses could be fed back from cortex or other subcortical structures. Taken together, these observations suggest that the vast majority (>80%) of geniculate inputs to layer 4C – and possibly all of the inputs to layer 4Cβ – are completely monocular in that the LGN neurons that send these axonal projections do not modulate under binocular viewing in primates. Our finding that effectively all monocular layer 4C neurons in our sample were binocularly modulated speaks for a cortical origin of this modulation.

METHODS

Surgical procedures: Two adult monkeys (*Macaca radiata,* one female*)* were used in this study. All procedures followed regulations by the Association for the Assessment and Accreditation of Laboratory Animal Care (AAALAC), Vanderbilt University's Institutional Animal Care and Use Committee (IACUC), and National Institutes of Health (NIH) guidelines. Each monkey was implanted with a custom-designed plastic head holder and a plastic recording chamber (Crist Instruments) in two separate surgeries under sterile conditions. The animal was administered isoflurane anesthesia (1.5-2.0%) while vital signs, including blood pressure, heart rate, SpO_2,

CO_2, respiratory rate, and body temperature were continuously monitored. During surgery, the head holder or the recording chamber were attached to the skull using transcranial ceramic screws (Thomas Recording) and self-curing denture acrylic (Lang Dental Manufacturing). A craniotomy was performed over the perifoveal visual field representation of primary visual cortex in each monkey concurrent with the position of the recording chamber. Each monkey was given analgesics and antibiotics for post-surgical care.

Neurophysiological equipment: During each recording session, a linear multielectrode array (UProbe, Plexon Inc.; Vector Arrays, NeuroNexus) with 24 or 32 contacts with 0.1 mm inter-electrode spacing was inserted into V1. Extracellular voltage fluctuations (0.5 kHz to 30 kHz) were recorded inside an electromagnetic radio frequency-shielded booth. These signals were amplified, filtered, and digitized using a 128-channel Cerebus® Neural Signal Processing System (NSP; Blackrock Microsystems). Both a broadband (0.3Hz – 7.5kHz) signal sampled at 30 kHz and a low frequency-dominated signal (0.3 Hz – 500 Hz) sampled at 1 kHz was saved for offline analysis. The NSP also recorded the output of a photodiode signal (OSI Optoelectronics) placed on the monitor to track stimulus-related events at 30 kHz, the output of the eye tracking system (EyeLink II, SR Research or SensoMotoric Instruments) at 1 kHz, and digital event markers sent from the behavioral control system (MonkeyLogic, see below). The photodiode signal and event markers were used to align the neural data with visual and behavioral events.

Neurophysiological Analysis: All neurophysiological signals were extracted offline from the digitized broadband signal using custom written code in MATLAB (2016a; The Mathworks, Inc.), with the exception of local field potentials (LFP), which were recorded as a separate signal (the low frequency-dominated signal noted above). We extracted single-unit activity (SUA) with

KiloSort, an open-source unsupervised machine-learning algorithm for spike-sorting[52], using the default parameters for sorting and cluster merging. A major benefit of using KiloSort for extracting single-unit activity from linear multielectrode arrays is that neurons that produce a signal on more than one microelectrode are not counted more than once. For all clusters detected by KiloSort, we extracted +/- 1 ms of data around each spike time from the original broadband signal for each simultaneously recorded electrode contact. We averaged across impulses to create a spatiotemporal map of the spike waveform (time x electrode contacts). The region of the spatiotemporal waveform map that exceeded +/- 30% of maximum modulus had to span fewer than 3 microelectrode channels (0.3 mm) and 0.9 ms to be included in the study. Clusters that met these criteria were localized to the microelectrode with the largest amplitude. In agreement with the original authors of the software[52], we found that the resulting spike isolation was comparable if not superior to spikes isolated via conventional spike sorting techniques (see **Fig.1** for examples). Spike rates were downsampled to 1 kHz. For each unit, spike times were converted to a time-varying signal using 0 to represent time points without a spike and 1 for time points where a spike was detected. This time-varying signal was then convolved using a Poisson distribution resembling a postsynaptic potential[53], with the spike rate (R) computed at time (t):

$$R(t) = \left[1 - \exp\left(-\frac{t}{\tau_g}\right)\right] * \left[\exp\left(-\frac{t}{\tau_d}\right)\right]$$

where τ_g and τ_d are the time constants for growth and decay, respectively. Values of 1 and 20 for τ_g and τ_d respectively were used based on previous studies[54]. After convolution, the signal was multiplied by the sampling frequency to convert units to impulses per second.

Current source density (CSD) analysis was performed on the LFP signal using an estimate of the second spatial derivative appropriate for electrodes with multiple contact points[55]:

$$\mathrm{CSD}\ (t,c) = -\frac{x(t,c-z) + x(t,c+z) - 2x(t,c)}{z^2}$$

where *x* is the extracellular voltage recorded in Volts at time *t* from an electrode contact at position *c*, and *z* is the electrode inter-contact distance (0.1 mm). In order to yield CSD in units of current per unit volume, the resulting CSD from the formula above was multiplied by 0.4 S/mm as an estimate of cortical conductivity[56].

Laminar alignment: For each penetration with the linear multielectrode array, CSD analysis was used to resolve the bottom of the prominent initial current sink immediately following stimulus onset. CSD analysis of visual responses to brief visual stimulation have been shown to reliably indicate the location of the primary geniculate input to V1 (in granular layer 4C, or L4) by a distinct current sink that is thought to reflect the combined excitatory post-synaptic potentials of the initial retino-geniculate volley of activation[57,58]. MUA responses, or more precisely lack thereof, were used to identify electrode contacts that lie outside V1, either in the subdural space or the white matter below. Further, we excluded channels on the extreme ends of the array that did not exhibit a clear receptive field (see *Receptive Field Mapping*). After removing these channels, the location of the initial current sink was used to align and average data across electrode penetrations, resulting in 0.1 mm +/- 0.05mm resolution across the depth of V1[59-67]. For display, representations of CSD as a function of time and space were Gaussian-filtered (σ = 0.1). Microelectrode contacts were classified to be in supragranular, granular, or infragranular positions based on the CSD responses as well as neurophysiological criteria such as the power spectral density of the LFP across cortical depth, signal correlations of the LFP between all channel combinations, and stimulus-evoked MUA response. The supragranular to granular

boundary is more challenging to define based on these criteria and was instead set to 0.5 mm above the granular to infragranular boundary.

Visual stimulation: Stimuli were presented on a linearized CRT monitor with a refresh rate of either 60 Hz (resolution 1280 × 1024) or 85 Hz (resolution 1024 × 768). These visual stimuli were generated using custom-written code in MonkeyLogic[68] for MATLAB (R2012-2014, The MathWorks) on a PC (Dell, Windows 7 or Windows 10) with a NVIDIA graphics card. Animals viewed all stimuli through a custom-built mirror stereoscope that employed infrared-light passing cold mirrors (Edmund Optics). The animal, mirrors, and monitor were positioned so that the animal's right eye viewed stimuli presented on the right side of the monitor and the animal's left eye viewed stimuli on the left side of the monitor. To prevent light scatter from one side of the monitor to the opposing eye, a black, non-reflective septum was placed between the monitor and the back side of the mirrors, effectively dividing the left and right sides of the apparatus. An infrared-light sensitive camera, placed directly behind mirrors that allowed infrared light to pass, was used to track gaze position with commercially available eye tracking software (Eye Link II, SR Research). Gaze position was converted to an analog signal and inputted to MonkeyLogic/MATLAB (NIDAQ PCI-6229) at 1 kHz. At the beginning of each recording session, the stereoscope was calibrated to facilitate fusion of the left and right sides of the monitor using a behavioral task that relied on acquiring the same gaze position for corresponding locations on the left and right sides of the monitor[69,70]. To further aid fusion, an oval aperture was displayed at the edge of each half-screen.

Visual paradigms and task: Each animal was trained to fixate on a small (0.2 degrees of visual angle, dva) cross presented at the center of each eye's visual field, for several (< 5) seconds while stimuli were presented in the perifoveal visual field. In experiment one, the animals fixated on a

fixation cross for 300 ms before a sequence of up to five circular sinusoidal gratings appeared. Each grating was presented for at least 200 ms before an inter-stimulus interval of at least 200 ms. The gratings were randomly presented to either the left eye, right eye, or both eyes over the population receptive field location of the recorded neurons. The grating stimuli varied in orientation but were always presented at a Michelson contrast above 0.45 (mode = 0.9) and at constant spatial frequency (0.5-3 cyc./deg) within a session. If the animals successfully held fixation within a 1 dva radius around the fixation cross for the entire stimulus sequence, a small amount of liquid juice reward was delivered. If the animals broke fixation or blinked, the trial was aborted and a short timeout (1-5 s) was given before the start of the next trial. In experiment two, a separate paradigm was used to measure neuronal responses to stimuli of varying contrast levels in each eye. Similar to experiment one, the animals fixated on a fixation cross for 300 ms before a sequence of up to five circular sinusoidal gratings appeared. Each grating was presented for at least 200 ms before an inter-stimulus interval of at least 200 ms. Gratings could be presented to one eye (left or right, with 0% contrast in the other eye) or both eyes. The Michelson contrast of the stimulus in each eye was one of four levels (0, 0.225, 0.45, 0.9). The sine-wave gratings were presented at a constant spatial frequency (0.5-3 cyc./deg) within a session and their orientation was either at the neurons' estimated preferred orientation or the orientation orthogonal to this preferred orientation (in all cases, stimulus orientation was always identical between the eyes). The preferred orientation was determined based on the audible response as well as an online analysis of the multiunit responses to sine-wave gratings of varying orientations. If the preferred orientation varied across electrode channels, the dominating (most frequent) preferred orientation was picked. Just like in experiment one, if the animal successfully held fixation within a 1 dva radius around the fixation cross for the entire stimulus sequence, a

small amount of liquid juice reward was delivered. If the animal broke fixation or blinked, the trial was aborted and a short timeout (1-5 s) was given before the start of the next trial.

Receptive Field Mapping: Once the linear multielectrode array was appropriately positioned in cortex, a reverse correlation-like technique was used to map the receptive fields of the units under study. In each trial, the animals fixated while up to five circular Gabor-filtered static random noise patches appeared in sequence at pseudorandom locations within a pre-defined virtual grid of monitor locations. Each noise patch was displayed for 150 ms with an inter-stimulus interval of 150 ms. The size of each noise patch and the pre-defined grid, respectively, depended on the recording session. Typically, each session included a "coarse" phase to determine the general location of the receptive field and a subsequent "fine" mapping phase to hone in on the precise location of the receptive field. To determine the location of the receptive field, 3D Receptive Field Matrices (RFMs)[71] were used to create a map of each electrode channel's neuronal response magnitude for different points in visual space. For every multiunit or single-unit, the spiking response to each stimulus presentation was averaged across time, resulting in a single scalar value. These scalar values were converted to units of z-score. The retinotopic portion of the RFM corresponding to the stimulus location was filled with the z-score for every presentation. This procedure produced a 3D matrix two dimensions representing vertical and horizontal visual space and a third dimension representing the response magnitude for each unit. This third dimension was then averaged, producing a spatial map of the unit's mean response. Receptive field centers and extents were computed by fitting an oval to the largest, contiguous patch of the spatial map that exceeded 1 z-score.

Unit Inclusion and Ocularity: Following elimination of electrode contacts outside the limits of V1's gray matter (see *Laminar Alignment*), we applied a few more criteria to determine valid

neuronal responses. For experiment one, the dominant eye of each unit was defined as the eye that yielded the highest spike rate between 30 ms and 130 ms following stimulus onset when stimulated with a high contrast stimulus. To be included for further analysis, this response had to exceed a maximum of 5 spikes per second, be significantly larger than fixation baseline (baseline window: -50 ms to 0 ms, stimulus window: 30 ms to 200 ms, paired t-test, $p < .05$), and there had to be at least 15 successfully completed trials of each contralateral and ipsilateral eye stimulation. For experiment one, we compared responses to stimulus presentations in each eye without stimulation of the other eye. To quantitatively compare the magnitude of response to each eye for each unit, we calculated an ocularity index using the following formula:

$$ocularity\ index = \frac{contralateral\ eye\ response - ipsilateral\ eye\ response}{contralateral\ eye\ response + ipsilateral\ eye\ response}$$

where response was defined as the half-wave rectified, baseline-subtracted mean spike rate from onset of the dominant-eye response until 100 ms following this onset, or the end of the stimulation period (200 ms), whichever came first. As verified by visual inspection, this window flexibly captured the initial response of each unit, while reducing variability across units with respect to onset latency and variance in the late, sustained portion of the response. Onset of the dominant-eye response was determined by detecting the first time point throughout the stimulation window where most data points exceeded a threshold (defined as mean baseline firing plus two times the standard deviation of that baseline firing) while increasing in magnitude. In experiment two, only single units were analyzed. To be included in the single-unit pool, each unit had to have a significant response to the dominant eye (as in experiment one), exceed a maximum of 5 spikes per second mean firing rate, and there had to be at least ten trials of high contrast visual stimulation for each eye.

Eye movement analysis. Using the horizontal and vertical gaze position data collected with the eye tracking software, we extracted the onset times of microsaccades using the algorithm described by Engbert and Mergenthaler[72].

Statistics: Most statistical analyses were performed using MATLAB-based functions. The single-unit and multiunit distributions of ocularity indices were each fit to a Gaussian that was truncated at -1 and 1. A Chi-square goodness of fit was used to determine whether the truncated Gaussian approximated the data. The mean rectified ocularity index in the supragranular, granular, and infragranular compartments were compared using a one-way ANOVA for each single-unit and multiunit populations. Tukey's HSD post hoc tests were used to compare individual compartments. Monocular neuron responses to high contrast dominant eye only stimulation were compared to responses to high contrast binocular stimulation using two methods. First, one-tailed t-tests were computed at the trial level for the single unit example (window: response onset through the next 100 ms), and at the unit level using z-score transformed responses for the conservative and liberal groups (30 ms to 130 ms). Second, ROC analysis was used to determine whether there was a significant difference between responses to binocular and monocular stimulation for each unit using 10 ms bins of data, with a sliding window of 1 ms during the response period (30-190 ms). Statistical significance was determined by comparing the area under the curve to a bootstrapped distribution of area under the curve values computed on 10,000 repetitions of shuffled data.

Anatomical MRI: Animals were anesthetized using the same procedure as outlined under *Animal Care and Surgical Procedures*. Anesthetized animals were placed inside a Philips Achieva 7T

MRI scanner at the Vanderbilt University Institute of Imaging Science and remained anesthetized throughout the duration of the scan. Vital signs were monitored continuously. T1-weighted 3D MPRAGE scans were acquired with a 32-channel head coil equipped for SENSE imaging. Images were acquired using a 0.5mm isotropic voxel resolution with the following parameters: repetition time (TR) 5s, echo time (TE) 2.5ms, flip angle 7°.

ACKNOWLEDGMENTS

The authors would like to thank Dr. W. Zinke, S. Amemori, Dr. T. Apple, M. Feurtado, George-Durrett, K., Dr. A. Graybiel, N. Halper, P. Henry, M. Johnson, Dr. C. Jones, M. Maddox, L. McIntosh, Dr. A. Newton. J. Parker, C. Thompson, K. Torab, C. Subraveti, B. Williams and R. Williams for technical advice and assistance. This work was supported by a research grant from the National Eye Institute (1R01EY027402-01). K.D. and J.A.W. are supported by a National Eye Institute Training Grant (5T32 EY007135-23). A.M. is supported by a research grant of the Whitehall Foundation, a Career Starter grant by the Knights Templar Eye Foundation, and a Fellowship of the Alfred P. Sloan Foundation. The authors declare no competing financial interests.

AUTHOR CONTRIBUTIONS

K.D., M.A.C. and A.M conceptualized and designed the study. K.D, and M.A.C. trained animals and implemented the experiments. K.D., M.A.C. and J.A.W. collected neurophysiological data and preprocessed the data. K.D. performed the data analysis and prepared the figures for publication. K.D. and A.M. wrote the manuscript with input from other authors.

FIGURE LEGENDS

Figure 1. Ocular dominance distribution across V1 neurons is approximately normal. (a) Experiment 1: Visual stimuli were presented through a mirror stereoscope. On every presentation, a high contrast sine-wave grating was presented to either the left or right eye over the population receptive field location. (b) Three example single-unit responses to monocular stimulation from one recording session. Spike rasters (left) and averaged spike density functions (right) show responses to ipsilateral and contralateral eyes, respectively. Error bars denote twice the standard error on the mean (S.E.M.) (c) Distribution of ocularity indices for single units (top) and multiunits (bottom) across both animals. Distributions for both populations are approximately normal (single units, Chi-square goodness-of-fit, $p = 0.02$, $\chi^2 = 17.66$, d.f. = 8); (multiunits, Chi-square goodness-of-fit, $p = 2.25 \times 10^{-18}$, $\chi^2 = 104.37$, d.f. = 9).

Figure 2. Laminar distribution of ocular dominance shows most monocular spiking in layer 4C. (a) Number of single units and multiunits at each cortical depth (left) as well as the mean rectified ocularity index at each cortical depth for these multiunits and single units (right). Error bars denote 2*S.E.M. at each cortical depth. Black vertical bars indicate significant differences between the rectified ocularity indices of multiunits between laminar compartments (one-way ANOVA, $F(2,771) = 53.23$, $p = 2.22 \times 10^{-22}$; supragranular and infragranular layers, Tukey's HSD post-hoc test, $p = 9.56 \times 10^{-10}$, $N_{supragranular} = 255$, $N_{infragranular} = 189$; granular and infragranular layers, Tukey's HSD post-hoc test, $p = 9.56 \times 10^{-10}$, $N_{granular} = 330$, $N_{infragranular} = 189$). There was no significant difference between laminar compartments for single units at the $\alpha = .05$ (one-way ANOVA, $F(2,185) = 2.42$, $p = .09$). (b) Average CSD response to a full field 100 ms flash of white light. (c) Average CSD response to the onset of a sine-wave grating

covering the receptive field, presented to the dominant eye for that penetration. Dominant eye based on the mean ocularity index across multiunits for each penetration.

Figure 3. Monocular V1 neurons modulate under binocular stimulation.

(a) Experiment 2: Dominant eye viewed a sine-wave grating at 4 different contrast levels (0, 22.5 45, 90%) while the non-dominant viewed either a 0% or 90% contrast stimulus. (b) Example responses of monocular neuron to a high-contrast grating in dominant eye and in both eyes, and a lack of response to non-dominant eye stimulation using a 90% contrast stimulus (paired t-test, $t_{117} = 0.01$, $p = 0.99$). Error bars denote 2*SEM. Purple dots indicate time points of significance ($\alpha = .05, .1$) based on ROC analysis. (c-d) Average response of completely monocular neurons (N = 7) and monocular neurons (N = 16) to dominant eye, non-dominant eye, and binocular stimulation at high contrast show significant suppression under binocular stimulation (conservative group, one-tailed t-test, $t_{12} = 2.59$, $p = 0.012$; liberal group, one-tailed t-test, $t_{30} = 1.77$, $p = .043$). Error bars denote 2*SEM. Grey lines separate ROC analysis for each unit in sample. Only units not shown in (c) are shown in (d). (e) Average spiking response during monocular and binocular stimulation (90% contrast in non-dominant eye) for unit in (b) normalized between 0 and 1. Error bars denote bootstrapped upper bound of 95% confidence interval on the mean. (f-g) Same as in (e) except for completely monocular (N = 7) and monocular units (N = 16), respectively. (h) Maximum area under the curve with ROC analysis in the response period (see Methods) for each unit in conservative (black lines) and liberal groups. (i) Monocular neurons' locations (liberal group, green). (j) Binocular neuron responses recorded in same penetrations as monocular neurons to the non-dominant eye of those monocular neurons.

Dark line represents mean response to the non-dominant eyes, and lighter blue lines represent individual mean responses. Error bar indicates 2*SEM.

REFERENCES

1. Heesy, C. P. On the relationship between orbit orientation and binocular visual field overlap in mammals. *Anat Rec A Discov Mol Cell Evol Biol* **281,** 1104–1110 (2004).
2. Blake, R., Sloane, M. & Fox, R. Further developments in binocular summation. *Percept Psychophys* **30,** 266–276 (1981).
3. Harwerth, R. S. & Smith, E. L. Binocular summation in man and monkey. *Am J Optom Physiol Opt* **62,** 439–446 (1985).
4. Ohzawa, I. & Freeman, R. D. The binocular organization of simple cells in the cat's visual cortex. *J Neurophysiol* **56,** 221–242 (1986).
5. Ohzawa, I., DeAngelis, G. C. & Freeman, R. D. Encoding of binocular disparity by complex cells in the cat's visual cortex. *J Neurophysiol* **77,** 2879–2909 (1997).
6. Ohzawa, I., DeAngelis, G. C. & Freeman, R. D. The neural coding of stereoscopic depth. *Neuroreport* **8,** iii–xii (1997).
7. Freeman, R. D. 2015 Charles F. Prentice Medal Award Lecture: Neural Organization of Binocular Vision. *Optometry and vision science : official publication of the American Academy of Optometry* **94,** 931–938 (2017).
8. Sengpiel, F. & Blakemore, C. The neural basis of suppression and amblyopia in strabismus. **10 (Pt 2),** 250–258 (1996).
9. Cumming, B. G. & DeAngelis, G. C. The physiology of stereopsis. *Annu. Rev. Neurosci.* **24,** 203–238 (2001).
10. Parker, A. J. & Cumming, B. G. Cortical mechanisms of binocular stereoscopic vision. *Prog. Brain Res.* **134,** 205–216 (2001).
11. Livingstone, M. S. & Tsao, D. Y. Receptive fields of disparity-selective neurons in macaque striate cortex. *Nat Neurosci* **2,** 825–832 (1999).
12. Ding, J. & Sperling, G. A gain-control theory of binocular combination. *PNAS* **103,** 1141–1146 (2006).
13. Meese, T. S., Georgeson, M. A. & Baker, D. H. Binocular contrast vision at and above threshold. *Journal of Vision* **6,** 1224–1243 (2006).
14. Parker, A. J. Binocular depth perception and the cerebral cortex. *Nat Rev Neurosci* **8,** 379–391 (2007).
15. Repérant, J., Miceli, D., Vesselkin, N. P. & Molotchnikoff, S. The centrifugal visual system of vertebrates: a century-old search reviewed. *Int. Rev. Cytol.* **118,** 115–171 (1989).
16. Casagrande, V. A. & Boyd, J. D. The neural architecture of binocular vision. *Eye (Lond)* **10 (Pt 2),** 153–160 (1996).
17. Wiesel, T. N. & Hubel, D. H. Spatial and chromatic interactions in the lateral geniculate body of the rhesus monkey. *J Neurophysiol* **29,** 1115–1156 (1966).

18. Hubel, D. H. & Wiesel, T. N. Binocular interaction in striate cortex of kittens reared with artificial squint. *J Neurophysiol* **28,** 1041–1059 (1965).
19. Hubel, D. H. & Wiesel, T. N. Receptive fields and functional architecture of monkey striate cortex. *J. Physiol. (Lond.)* **195,** 215–243 (1968).
20. Mitzdorf, U. Current source-density method and application in cat cerebral cortex: investigation of evoked potentials and EEG phenomena. *Physiological Reviews* **65,** 37–100 (1985).
21. Douglas, R. J., Martin, K. A. C. & Whitteridge, D. A Canonical Microcircuit for Neocortex. *Neural Comput* **1,** 480–488 (1989).
22. Hubel, D. H. & Wiesel, T. N. Laminar and columnar distribution of geniculo-cortical fibers in the macaque monkey. **146,** 421–450 (1972).
23. Blasdel, G. G. & Fitzpatrick, D. Physiological organization of layer 4 in macaque striate cortex. *J. Neurosci.* **4,** 880–895 (1984).
24. Ahmed, B., Anderson, J. C., Douglas, R. J., Martin, K. A. & Nelson, J. C. Polyneuronal innervation of spiny stellate neurons in cat visual cortex. *J. Comp. Neurol.* **341,** 39–49 (1994).
25. Binzegger, T., Douglas, R. J. & Martin, K. A. C. A quantitative map of the circuit of cat primary visual cortex. *Journal of Neuroscience* **24,** 8441–8453 (2004).
26. Chadnova, E., Reynaud, A., Clavagnier, S. & Hess, R. F. Short-term monocular occlusion produces changes in ocular dominance by a reciprocal modulation of interocular inhibition. *Sci Rep* **7,** 41747 (2017).
27. Mineault, P. J., Zanos, T. P. & Pack, C. C. Local field potentials reflect multiple spatial scales in V4. *Front Comput Neurosci.* **7,** 21 (2013).
28. Wiesel, T. N., Hubel, D. H. & Lam, D. M. Autoradiographic demonstration of ocular-dominance columns in the monkey striate cortex by means of transneuronal transport. *Brain Res.* **79,** 273–279 (1974).
29. Florence, S. L. & Kaas, J. H. Ocular dominance columns in area 17 of Old World macaque and talapoin monkeys: complete reconstructions and quantitative analyses. *Vis. Neurosci.* **8,** 449–462 (1992).
30. Horton, J. C. & Hocking, D. R. Intrinsic variability of ocular dominance column periodicity in normal macaque monkeys. *J. Neurosci.* **16,** 7228–7239 (1996).
31. Blake, R. A neural theory of binocular rivalry. *Psychol Rev* **96,** 145–167 (1989).
32. Read, J. C. A., Parker, A. J. & Cumming, B. G. A simple model accounts for the response of disparity-tuned V1 neurons to anticorrelated images. *Vis. Neurosci.* **19,** 735–753 (2002).
33. Said, C. P. & Heeger, D. J. A model of binocular rivalry and cross-orientation suppression. *PLoS Comput Biol* **9,** e1002991 (2013).
34. Kato, H., Bishop, P. O. & Orban, G. A. Binocular interaction on monocularly discharged lateral geniculate and striate neurons in the cat. *J Neurophysiol* **46,** 932–951 (1981).
35. Dougherty, K., Schmid, M. C. & Maier, A. Binocular Response Modulation in the Lateral Geniculate Nucleus. *J. Comp. Neurol.* (2018). doi:10.1002/cne.24417
36. Schiller, P. H., Finlay, B. L. & Volman, S. F. Quantitative studies of single-cell properties in monkey striate cortex. II. Orientation specificity and ocular dominance. *J Neurophysiol* **39,** 1320–1333 (1976).

37. Kiorpes, L., Kiper, D. C., O'Keefe, L. P., Cavanaugh, J. R. & Movshon, J. A. Neuronal correlates of amblyopia in the visual cortex of macaque monkeys with experimental strabismus and anisometropia. *J. Neurosci.* **18,** 6411–6424 (1998).
38. Baker, F. H., Grigg, P. & Noorden, von, G. K. Effects of visual deprivation and strabismus on the response of neurons in the visual cortex of the monkey, including studies on the striate and prestriate cortex in the normal animal. *Brain Res.* **66,** 185–208 (1974).
39. Blasdel, G. G. & Lund, J. S. Termination of afferent axons in macaque striate cortex. *J. Neurosci.* **3,** 1389–1413 (1983).
40. Katz, L. C., Gilbert, C. D. & Wiesel, T. N. Local circuits and ocular dominance columns in monkey striate cortex. *J Neurosci* (1989).
41. Gilbert, C. D. & Wiesel, T. N. Columnar specificity of intrinsic horizontal and corticocortical connections in cat visual cortex. **9,** 2432–2442 (1989).
42. Gilbert, C. D. & Wiesel, T. N. Intrinsic connectivity and receptive field properties in visual cortex. *Vision Research* **25,** 365–374 (1985).
43. Moradi, F. & Heeger, D. J. Inter-ocular contrast normalization in human visual cortex. *Journal of Vision* **9,** 13.1–22 (2009).
44. Sanderson, K. J., Bishop, P. O. & Darian-Smith, I. The properties of the binocular receptive fields of lateral geniculate neurons. *Exp Brain Res* **13,** 178–207 (1971).
45. Pape, H. C. & Eysel, U. T. Binocular interactions in the lateral geniculate nucleus of the cat: GABAergic inhibition reduced by dominant afferent activity. *Exp Brain Res* **61,** 265–271 (1986).
46. Singer, W. Inhibitory binocular interaction in the lateral geniculate body of the cat. *Brain Res.* **18,** 165–170 (1970).
47. Schmielau, F. & Singer, W. The role of visual cortex for binocular interactions in the cat lateral geniculate nucleus. *Brain Res.* **120,** 354–361 (1977).
48. Varela, F. J. & Singer, W. Neuronal dynamics in the visual corticothalamic pathway revealed through binocular rivalry. *Exp Brain Res* **66,** 10–20 (1987).
49. Rodieck, R. W. & Dreher, B. Visual suppression from nondominant eye in the lateral geniculate nucleus: a comparison of cat and monkey. *Exp Brain Res* **35,** 465–477 (1979).
50. Cheong, S. K., Tailby, C., Solomon, S. G. & Martin, P. R. Cortical-like receptive fields in the lateral geniculate nucleus of marmoset monkeys. *Journal of Neuroscience* **33,** 6864–6876 (2013).
51. Zeater, N., Cheong, S. K., Solomon, S. G., Dreher, B. & Martin, P. R. Binocular Visual Responses in the Primate Lateral Geniculate Nucleus. *Curr. Biol.* **25,** 3190–3195 (2015).
52. Pachitariu, M., Steinmetz, N., Kadir, S., Carandini, M. & Harris, K. D. Kilosort: realtime spike-sorting for extracellular electrophysiology with hundreds of channels. 1–14 (2016). doi:10.1101/061481
53. Sayer, R. J., Friedlander, M. J. & Redman, S. J. The time course and amplitude of EPSPs evoked at synapses between pairs of CA3/CA1 neurons in the hippocampal slice. *J. Neurosci.* **10,** 826–836 (1990).
54. Hanes, D. P., Thompson, K. G. & Schall, J. D. Relationship of presaccadic activity in frontal eye field and supplementary eye field to saccade initiation in macaque: Poisson spike train analysis. *Exp Brain Res* **103,** 85–96 (1995).

55. Nicholson, C. & Freeman, J. A. Theory of current source-density analysis and determination of conductivity tensor for anuran cerebellum. *J Neurophysiol* **38,** 356–368 (1975).
56. Logothetis, N. K., Kayser, C. & Oeltermann, A. In vivo measurement of cortical impedance spectrum in monkeys: implications for signal propagation. **55,** 809–23 (2007).
57. Mitzdorf, U. & Singer, W. Laminar segregation of afferents to lateral geniculate nucleus of the cat: an analysis of current source density. *J Neurophysiol* **40,** 1227–1244 (1977).
58. Schroeder, C. E., Mehta, A. D., Givre, S. J. & Schroeder, C. A spatiotemporal profile of visual system activation revealed by current source density analysis in the awake macaque. *Cereb. Cortex* **8,** 575–592 (1998).
59. Maier, A., Adams, G. K., Aura, C. & Leopold, D. A. Distinct superficial and deep laminar domains of activity in the visual cortex during rest and stimulation. *Front Syst Neurosci* **4,** (2010).
60. Maier, A., Aura, C. J. & Leopold, D. A. Infragranular sources of sustained local field potential responses in macaque primary visual cortex. *Journal of Neuroscience* **31,** 1971–1980 (2011).
61. Godlove, D. C., Maier, A., Woodman, G. F. & Schall, J. D. Microcircuitry of agranular frontal cortex: testing the generality of the canonical cortical microcircuit. *Journal of Neuroscience* **34,** 5355–5369 (2014).
62. Spaak, E., Bonnefond, M., Maier, A., Leopold, D. A. & Jensen, O. Layer-specific entrainment of gamma-band neural activity by the alpha rhythm in monkey visual cortex. *Current Biology* **22,** 2313–8 (2012).
63. Dougherty, K., Cox, M. A., Ninomiya, T., Leopold, D. A. & Maier, A. Ongoing Alpha Activity in V1 Regulates Visually Driven Spiking Responses. *Cereb. Cortex* bhv304 (2015). doi:10.1093/cercor/bhv304
64. van Kerkoerle, T. *et al.* Alpha and gamma oscillations characterize feedback and feedforward processing in monkey visual cortex. *PNAS* **111,** 14332–14341 (2014).
65. Hansen, B., Chelaru, M. & Dragoi, V. Correlated Variability in Laminar Cortical Circuits. *Neuron* **76,** 590–602 (2012).
66. Ninomiya, T., Dougherty, K., Godlove, D. C., Schall, J. D. & Maier, A. Microcircuitry of agranular frontal cortex: contrasting laminar connectivity between occipital and frontal areas. *J Neurophysiol* jn.00624.2014 (2015). doi:10.1152/jn.00624.2014
67. Cox, M. A. *et al.* Spiking Suppression Precedes Cued Attentional Enhancement of Neural Responses in Primary Visual Cortex. *Cereb. Cortex* **97,** 1–14 (2017).
68. Asaad, W. F., Santhanam, N., McClellan, S. & Freedman, D. J. High-performance execution of psychophysical tasks with complex visual stimuli in MATLAB. *J Neurophysiol* **109,** 249–260 (2013).
69. Maier, A., Logothetis, N. K. & Leopold, D. A. Context-dependent perceptual modulation of single neurons in primate visual cortex. *PNAS* **104,** 5620–5625 (2007).
70. Maier, A. *et al.* Divergence of fMRI and neural signals in V1 during perceptual suppression in the awake monkey. *Nat Neurosci* **11,** 1193–1200 (2008).
71. Cox, M. A. *et al.* Receptive field focus of visual area V4 neurons determines responses to illusory surfaces. *PNAS* **110,** 17095–17100 (2013).
72. Engbert R. & Mergenthaler K. Microsaccades are triggered by low retinal image slip. *PNAS*. **103**, 7192-7 (2006).

Table 1. Individual statistics for each monocular neuron. Paired t-tests were computed for each unit on the non-dominant eye using a baseline period (-50-0 ms, relative to stimulus onset) and a response period (30-130 ms).

UNIT	non-dominant eye p-value	non-dominant eye t-statistic	non-dominant eye d.f.	ocularity index
1	0.83	-0.21	113	-1.00
2	0.12	-1.60	66	-1.00
3	0.17	-1.38	96	-0.73
4	0.53	0.63	81	0.90
5	0.99	0.01	117	0.85
6	0.84	0.20	115	0.65
7	0.76	0.31	127	0.40
8	0.12	1.59	48	1.00
9	0.09	1.71	120	-0.77
10	0.14	1.48	171	-0.87
11	0.04	2.11	137	0.83
12	0.59	-0.54	116	0.79
13	0.18	1.36	190	-0.68
14	0.21	1.28	80	0.77
15	0.09	1.59	113	-0.88

Figure 1

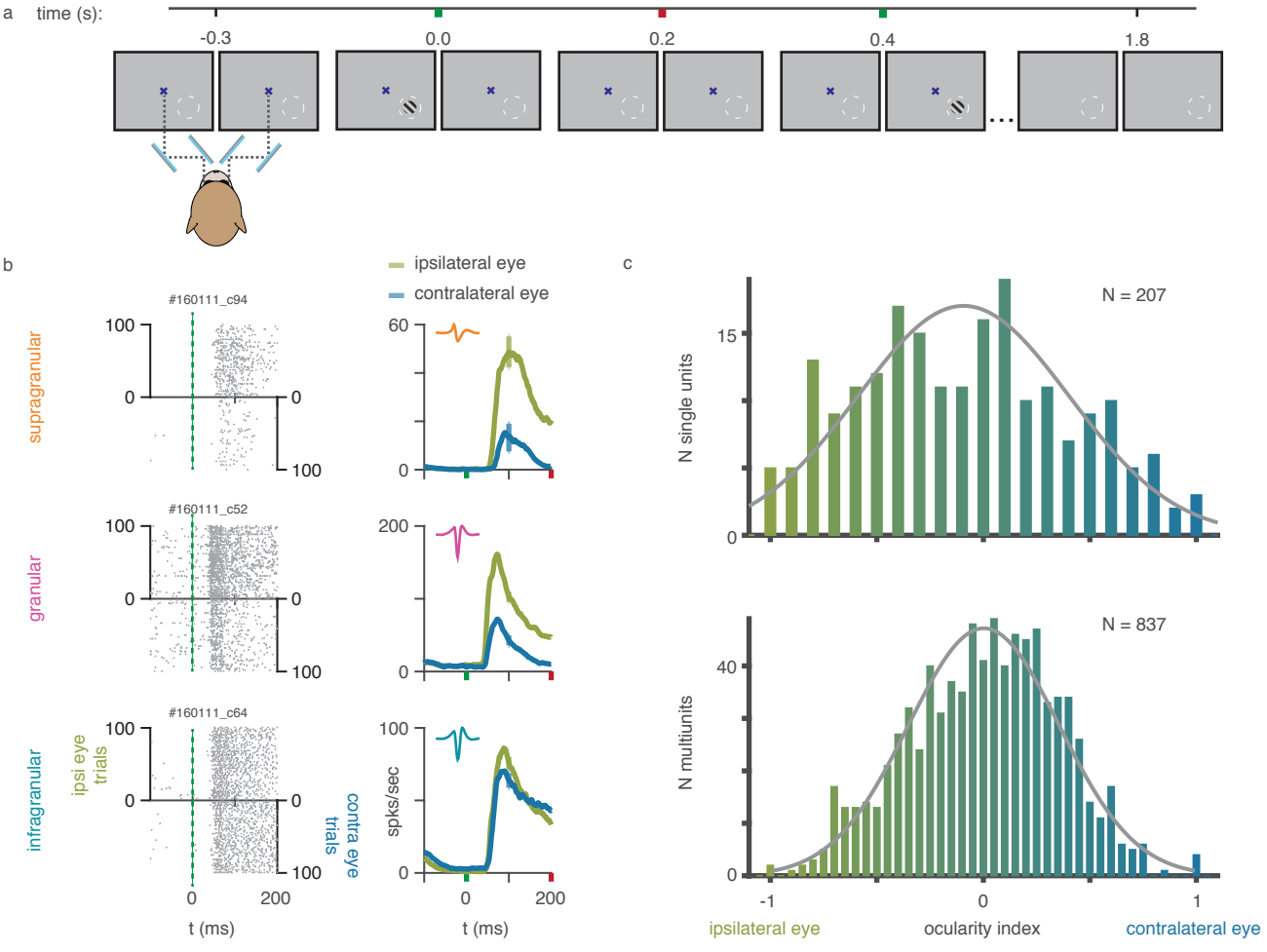
a
time (s):
-0.3
0.0
0.2
0.4
1.8
b
ipsilateral eye
contralateral eye
supragranular
granular
infragranular
#160111_c94
#160111_c52
#160111_c64
ipsi eye trials
contra eye trials
spks/sec
t (ms)
c
N = 207
N = 837
N single units
N multiunits
ipsilateral eye
ocularity index
contralateral eye

Figure 2

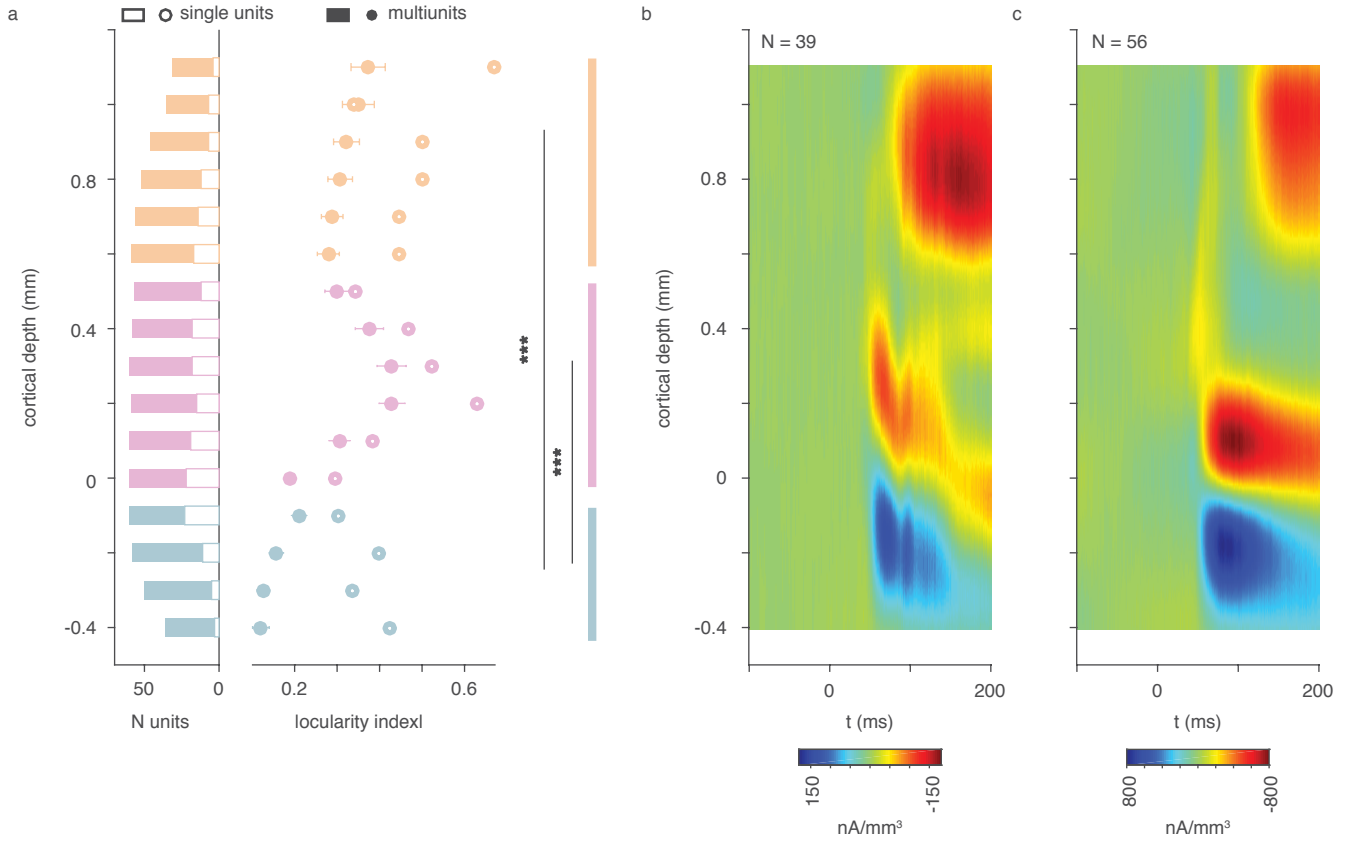
a
single units
multiunits
cortical depth (mm)
0.8
0.4
0
-0.4
50
0
N units
0.2
0.6
locularity indexl
***
***
b
N = 39
cortical depth (mm)
0.8
0.4
0
-0.4
0
200
t (ms)
150
-150
nA/mm³
c
N = 56
0
200
t (ms)
800
-800
nA/mm³

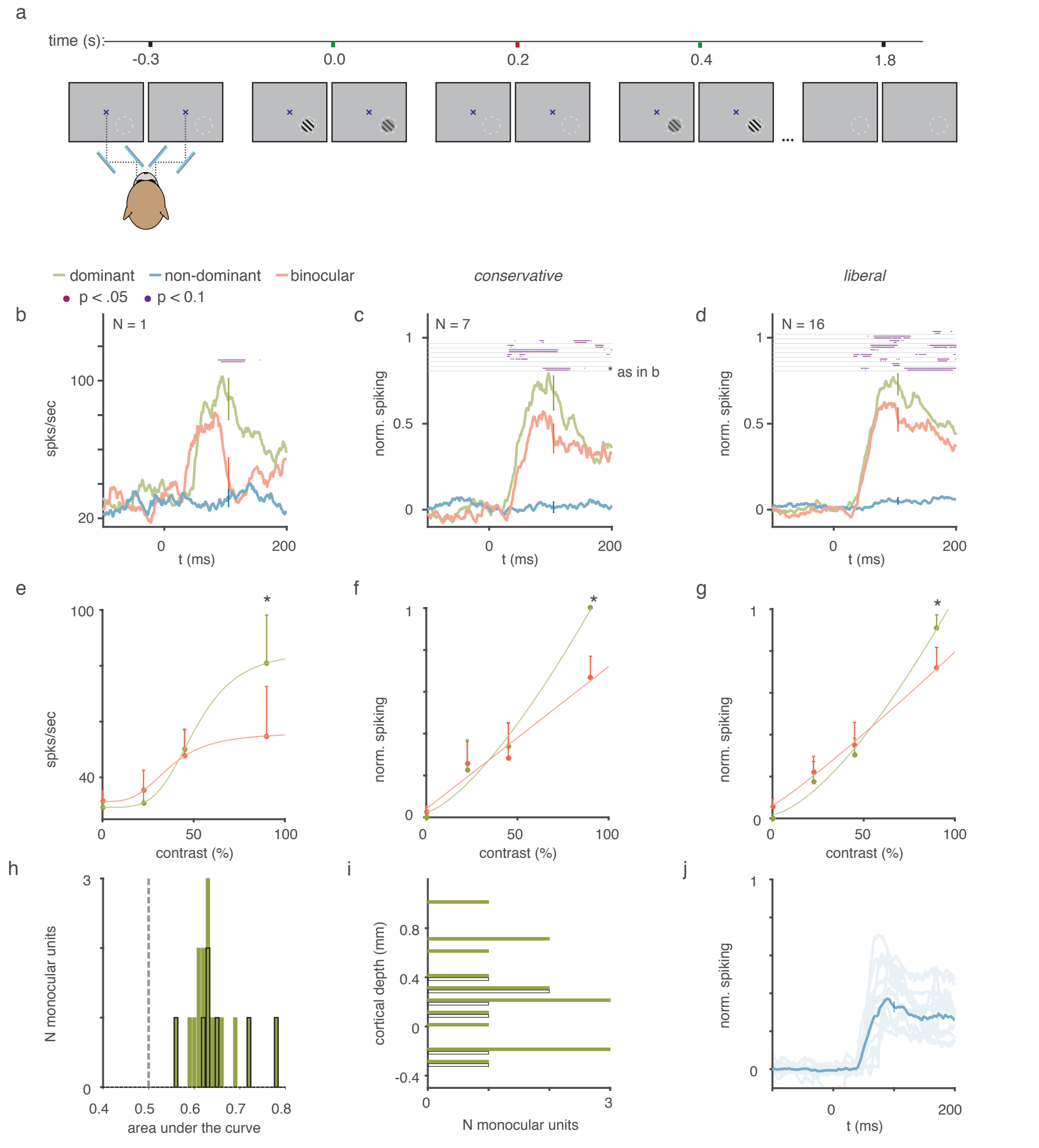
a
time (s):
-0.3
0.0
0.2
0.4
1.8
dominant
non-dominant
binocular
p < .05
p < 0.1
conservative
liberal
b
N = 1
spks/sec
100
20
0
200
t (ms)
c
N = 7
norm. spiking
1
0.5
0
* as in b
d
N = 16
e
f
g
contrast (%)
h
N monocular units
area under the curve
i
cortical depth (mm)
0.8
0.4
-0.4
j